Design and experimental validation of an adaptive phononic crystal using highly dissipative polymeric material interface

K. Billon[a], M. Ouisse[a], E. Sadoulet-Reboul[a], M. Collet[b], G. Chevallier[a], and A. Khelif[a]

[a]Univ. Bourgogne Franche-Comté FEMTO-ST Institute CNRS/UFC/ENSMM/UTBM, Department of Applied Mechanics, 24 chemin de l'Epitaphe, 25000 Besançon, France
[b]Laboratory of Tribology and Systems Dynamics (LTDS), École Centrale de Lyon, 36 avenue Guy de Collongue, 69134 Ecully, France

ABSTRACT

In this paper, some numerical tools for dispersion analysis of periodic structures are presented, with a focus on the ability of the methods to deal with dissipative behaviour of the systems. An adaptive phononic crystal based on the combination of metallic parts and highly dissipative polymeric interface is designed. The system consists in an infinite periodic bidirectional waveguide. The periodic cylindrical pillars include a layer of shape memory polymer and Aluminum. The mechanical properties of the polymer depend on both temperature and frequency and can radically change from glassy to rubbery state, with various combination of high/low stiffness and high/low dissipation. A fractional derivative Zener model is used for the description of the frequency-dependent behaviour of the polymer. A 3D finite element model of the cell is developed for the design of the metamaterial. The "Shifted-Cell Operator" technique consists in a reformulation of the PDE problem by "shifting" in terms of wave number the space derivatives appearing in the mechanical behaviour operator inside the cell, while imposing continuity boundary conditions on the borders of the domain. Damping effects can easily be introduced in the system and a quadratic eigenvalue problem yields to the dispersion properties of the periodic structure. In order to validate the design and the adaptive character of the metamaterial, results issued from a full 3D model of a finite structure embedding an interface composed by a distributed set of the unit cells are presented. Various driving temperature are used to change the behaviour of the system. After this step, a comparison between the results obtained using the tunable structure simulation and the experimental results is presented. Two states are obtained by changing the temperature of the polymeric interface: at $25°C$, the bandgap is visible around a selected frequency. Above the glass transition, the phononic crystal tends to behave as an homogeneous plate.

Keywords: Periodic structures, Metamaterial, Dispersion, Dissipation, Vibroacoutic.

1. INTRODUCTION

A periodic medium is a material or a structural system that exhibits spatial periodicity.[1] The study of periodic structures has a long history in the field of vibrations and acoustics.[2] This topic has interested researchers over the years, and a growing activity on this field is observed on the last years, with the objective of designing structures exhibiting properties that conventional ones cannot possess.[3–5] The methods currently used are most of the time based on those derived from wave propagation in crystals,[6] where almost no dissipation occurs. Reaching the upper scale for structural dynamics implies that damping effects have to be included in the analyses which are performed.

2. METAMATERIAL DESIGN

The system consists in an infinite periodic bidirectional waveguide shown in figure 1a. All sollicitations are considered. It is a 1 mm thick plate with periodic cylindrical pillars. Due to the periodicity, the unit cell is used and the corresponding first Brillouin zone is described in figure 1b.

Further author information: (Send correspondence to Morvan Ouisse)
E-mail: morvan.ouisse@femto-st.fr, Telephone: +33 3 81 66 60 00

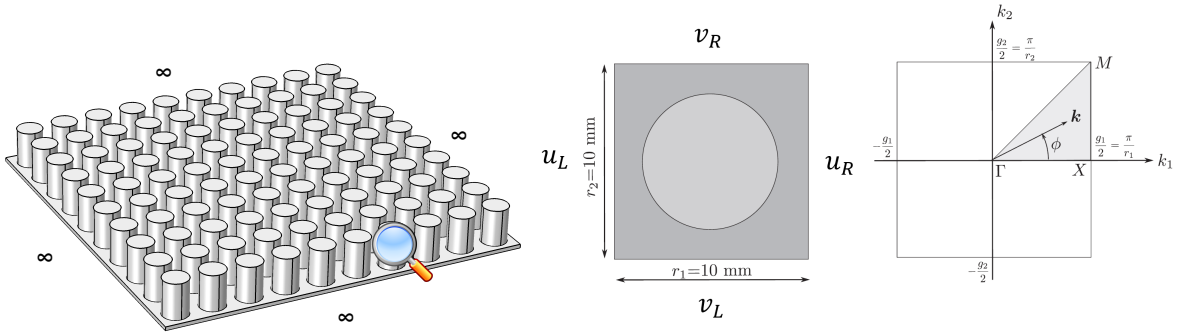

(a) (b)

Figure 1. a) Infinite wave guide. b) Real and reciprocal lattices.

In order to design a two-state phononic crystal, a polymeric base is included in the pillar (figure 2). The base plate is made of isotropic Aluminium 6063-T83 ($\nu = 0,33, E = 69\ GPa$ and $\rho = 2700\ kg/m^3$). Pillars are made of combination between a highly dissipative polymer tBA/PEGDMA ($\nu_{poly} = 0,37, E_{poly}$, defined in the following and $\rho_{poly} = 1004[kg/m^3]$)[7] and Aluminum 6063-T83.

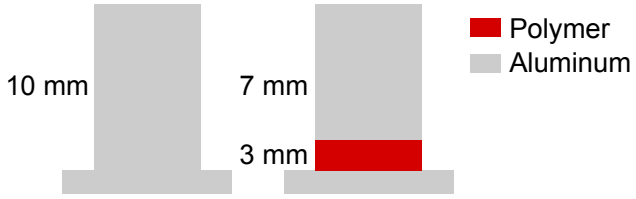

(a) (b)

Figure 2. a) Reference structure, 10 mm height aluminum cylinder. b) Metamaterial with 3 mm height polymeric interface between base and 7 mm height aluminum cylinder.

The polymer thickness has been chosen in order to open a resonant bandgap under the bragg bandgap frequency According to the manufacturing process, the maximum thickness obtained after the UV photopolymerization is 3 mm. Let assume that the polymer behaviour is like a 1D spring-mass system, the natural frequency can be defined as

$$f_0 = \frac{\sqrt{\frac{K_{poly}}{M_{alu}}}}{2\pi} \tag{1}$$

with $K_{poly} = \frac{E_{poly}S}{h_{poly}}$ and $M_{alu} = \rho_{alu}Sh_{alu}$ where S is the cylinder section, h_{poly} and h_{alu} respectively the polymer thickness and the aluminium thickness. This frequency is around 40 kHz in this case.

A suitable model is required for the description of the frequency-dependent behaviour of the polymer. In the harmonic regime, the Young's modulus of the polymer is complex, dependent on frequency and temperature,

$$E^*_{poly}(\omega, T) = E' + jE'' = E' \times (1 + j \times tan(\delta)), \tag{2}$$

where $tan(\delta) = E''/E'$ is the loss factor, E' is the storage modulus and E'' is the loss modulus. In this work, a fractional derivative Zener model is used. Moreover this material exhibits a strong temperature dependency that will be used to obtain the two-state phononic crystal. The expression of the elastic complex modulus is

$$E^*_{poly}(\omega, T) = \frac{E_{0poly} + E_{\infty poly}(j\omega\tau(T))^\alpha}{1 + (j\omega\tau(T))^\alpha}, \tag{3}$$

where E_{0poly} et $E_{\infty poly}$ are respectively the static elastic modulus and the high-frequency limit value of the dynamical modulus, τ is the relaxation time and is the order of fractional derivative. An estimation of the four parameters E_{0poly}, $E_{\infty poly}$, α and τ are obtained by experimental measurements.[8]

Three damping configurations are studied, one with low damping at ambient temperature, one with high dissipation at $90°C$ and an intermediate one at $60°C$. At ambient temperature, the polymer is stiff and its loss factor is almost equal to zero. At $90°C$, the loss factor is over 1.5 on the frequency range (0 to $100kHz$), with a maximum value of 2.5. At $60°C$, the intermediate configuration, damping remains high at low frequencies and decrease to reach high frequencies. The storage modulus and loss factor are plotted in figure 3a and figure 3b. The blue line is associated to the ambient temperature, the red one to $60°C$ and finally the yellow one to $90°C$.

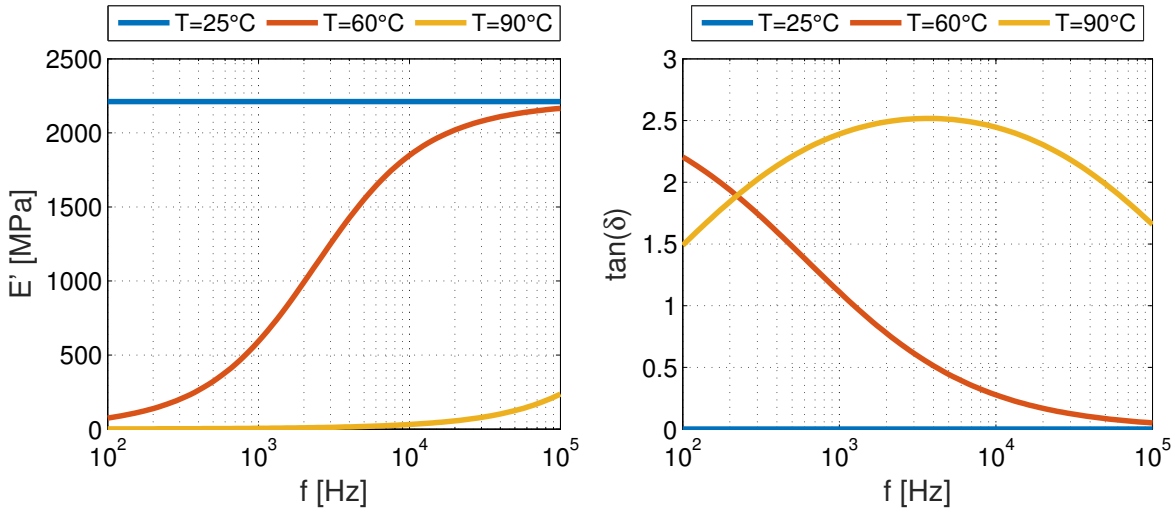

(a) (b)

Figure 3. a) Storage modulus. b) tBA/PEGDMA loss factor for several temperature, $25°C$, $60°C$ and $90°C$ respectively in blue, red and yellow.

3. DYNAMICAL PROPERTIES

3.1 Dispersion analysis

The "Shifted-Cell Operator" technique consists in reformulating the PDE problem by "shifting" in terms of wave number the space derivatives appearing in the mechanical behaviour operator inside the cell, while imposing continuity boundary conditions on the borders of the domain. The formulation leads to the following eigenvalue problem[9] :

$$[(\mathbf{K} - \omega^2\mathbf{M}) + \lambda_i(\mathbf{L} - \mathbf{L}^T) - \lambda_i^2\mathbf{H}]\boldsymbol{\phi}_i^r = 0, \tag{4}$$

where $\lambda_i = jk_i$ is the $i-th$ eigenvalue, $\boldsymbol{\phi}_i^r$ denotes the right eigenvector associated to λ_i, $\mathbf{M}$ and $\mathbf{K}$ are respectively the standard symmetric definite mass and symmetric semi-definite stiffness matrices, $\mathbf{L}$ is a skew-symmetric matrix and $\mathbf{H}$ is a symmetric semi-definite positive matrix. In this formulation, all matrices can depend on ω. A parametric eigenvalue analysis is then performed where the pulsation ω is fixed as real parameter, allowing introduction of damping effects. The wavenumbers $\lambda_i = jk_i$ and the associated right eigenvectors $\boldsymbol{\phi}_i^r$ are computed by solving the quadratic eigenvalue problem.

For frequency-dependent systems, the estimation of the group velocity is not trivial.[10,11] We focus on homogeneous cases where the frequency dependency is characterized by a Young's modulus such that $E = f(\omega)E_0$ and a constant Poisson's ratio. Hence $\mathbf{K} = f(\omega)\mathbf{K}_0$, $\mathbf{H} = f(\omega)\mathbf{H}_0$ et $\mathbf{L} = f(\omega)\mathbf{L}_0$. In this case we obtain

$$C_g = real\left(\frac{\partial \omega}{\partial k_i}\right) = real\left(\frac{j\boldsymbol{\phi}_i^{l^T}[f(\omega)(-\mathbf{L}_0 + \mathbf{L}_0^T + 2\lambda_i \mathbf{H}_0)]\boldsymbol{\phi}_i^r}{\boldsymbol{\phi}_i^{l^T}[\omega^2 \frac{\frac{\partial f}{\partial \omega}}{f(\omega)} - 2\omega]\mathbf{M}\boldsymbol{\phi}_i^r}\right). \tag{5}$$

The "Shifted-Cell Operator" technique is used to obtain dispersion curves along the $\Gamma - X$ direction. Damping is included in the analyses due to complex polymer Young's modulus using fractional derivative Zener model.

Figures 4a to 4c show dispersion curves along the $\Gamma - X$ direction obtained with the "Shift cell operator" method. A comparison between the results obtained using the reference structure and the tunable structure is presented. The two states are obtained by changing the temperature of the polymeric interface: at $25°C$, the bandgap is visible around the selected frequency ($40\ kHz$) linked to the design of the resonator. Above the glass transition, the phononic crystal tends to behave as an homogeneous plate.

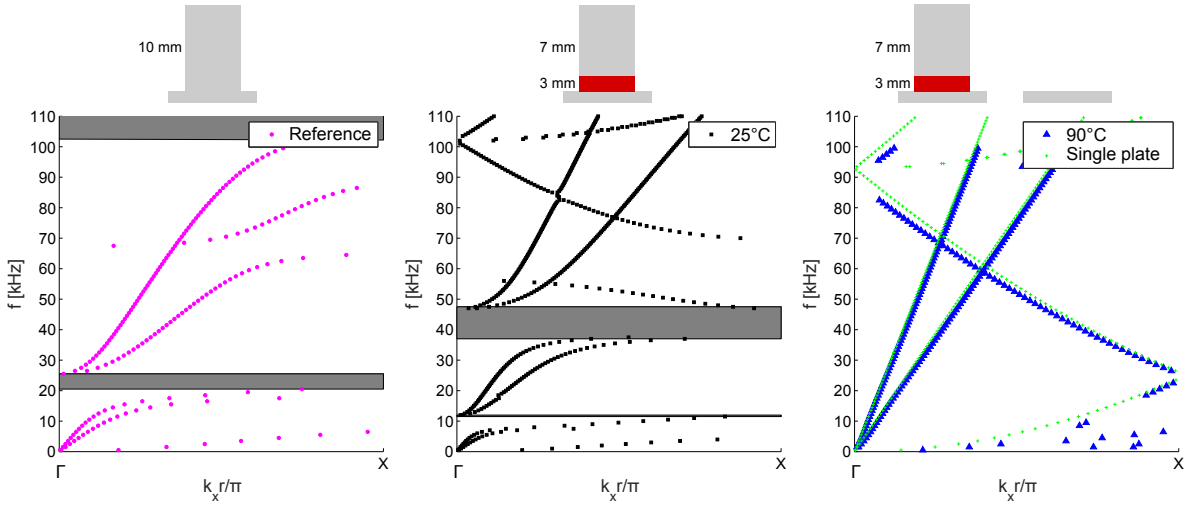

(a) (b) (c)

Figure 4. Dispersion curves along the $\Gamma - X$ direction obtained with the "Shift cell operator" method. a) Reference structure, all in aluminum. b) Metamaterial at ambient temperature $25°C$. c) Metamaterial at $90°C$ et aluminum plate.

3.2 Finite structure

The main goal of this part is to validate in a finite structure the phenomenon observed on an infinite structure. A finite element model is presented. This is followed by an experimental validation. The metamaterial ($21 \times 7 \times 0.1\ cm^3$) includes an interface composed by 7×7 unit cells (figure 5).

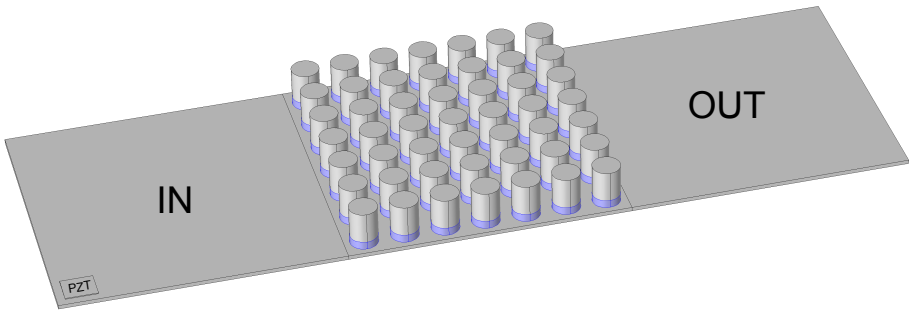

Figure 5. Finite structure with an interface composed by 7×7 unit cells distributed. Piezoelectric patch (PZT) for excitation in the bottom left corner.

The three temperatures are studied and the metamaterial is free. A piezoelectric patch with harmonic voltage ($|U| = 100\ V$) is incluted in the model in order to be close to the experimental set up and cover all the frequency range from 0 to 50 kHz. Figure 6 shows numerical frequency responses obtained with the finite elements code. Squared velocity amplitudes $|Vz|^2$ are averaged for the input plate (IN) and the output plate (OUT). Blue and red curves are numerical frequency response at ambient temperature $25°C$ for the input plate (IN) and the output plate (OUT). Yellow and purple curves at $90°C$. The grey shape represents the bandgap predicted by the dispersion analyses at ambient temperature.

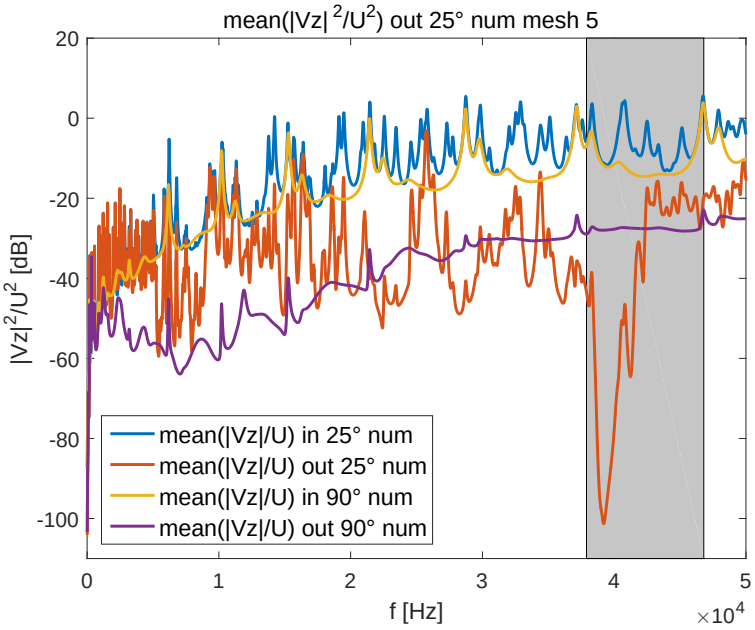

Figure 6. Numerical frequency responses. Average squared velocity amplitude $|Vz|^2$ for the input plate (IN) and the output plate (OUT) at ambient temperature $25°C$ respectively in blue and red. At $90°C$, respectively in yellow and purple. The grey shape represents the bandgap predicted by the dispersion analyses at ambient temperature.

At ambient temperature $25°C$, an output attenuation around 40 kHz is observed smaller than the frequency range predicted by bandgap. This is due to the boundary conditions. After shapes analyses, edge modes propagates along each edges of the periodic lattice. At $90°C$, after the glass transition, the output attenuation is not visible anymore.

3.3 Experimental validation

The metamaterial is made of metal and polymer. Polymer parts are realised by laser cutting and metallic part by classical mechanical processing (figure 7). The metamaterial is assembled in two steps by bonding parts together. Polymer cylinders are sticked on the support plate. After drying and load process, at ambient temperature during 24 hours, aluminum cylinders are sticked on polymer cylinders. Piezoelectric patch provides harmonic excitation up to 50 kHz.

Figure 8a illustrates experimental facility composed by :

- the metamaterial with his mounting bracket,
- a thermal chamber,
- a 3D vibrometer,
- a piezoelectric amplifier

Figure 7. Metamaterial after several manufacturing steps.

- and a thermocouple.

The metamaterial is suspended thanks to a mounting bracket to reproduce free boundary condition (figure 8b). The mounting bracket is introduced in a thermal chamber which presents a glass wall required for 3D vibrometer measurements.

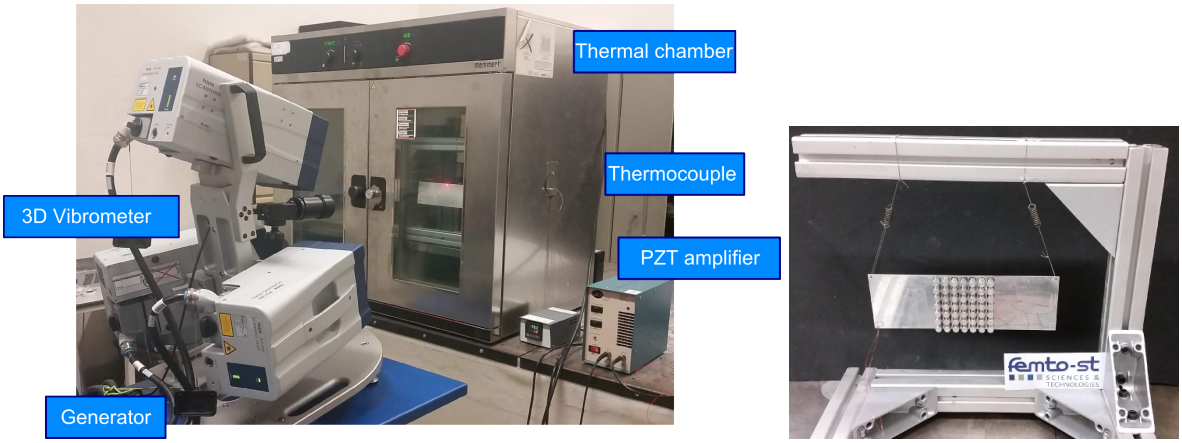

(a) (b)

Figure 8. a) Experimental facility with the main equipment as the metamaterial, the 3D vibrometer and the thermal chamber; b) A zoom is done on the metamaterial with free boundary conditions.

The white noise generator provides random harmonic voltage (5 V) between 500Hz and 50kHz, this signal is amplified 20 times by the piezoelectric amplifier. Temperatures are selected using the thermal chamber and controlled by the thermocouple. The 3D vibrometer is used to measure the velocity and frequency responses are calculated with $H1$ estimator.

Figure 9a presents numerical and experimental frequency responses at ambient temperature $25°C$. Curves need to be compared by pair (yellow-blue and purple-red). Yellow and blue curves corresponds, respectively, to experimental and numerical average squared velocity amplitude $|Vz|^2$ for the input plate (IN). Purple and red curves corresponds, respectively, to experimental and numerical average squared velocity amplitude $|Vz|^2$ for the output plate (OUT). In the bandgap region, attenuation predicted by numerical simulation is around 100dB, which corresponds to a ratio between output and input squared velocity amplitude equal to 10^5. Numerical amplitudes are considerably lower than experimental amplitudes taking into account experimental environment. Experimental facilities do not lead us to reach the same measurement dynamic. The noise level estimation is done and the green curve shows the noise generated by the surrounding equipments (acquisition chain, room fan). In any case, it is impossible to measure vibrating levels below this limit. The general trends (yellow-blue and purple-red) are similar except in areas where the measurement is close to ambient noise.

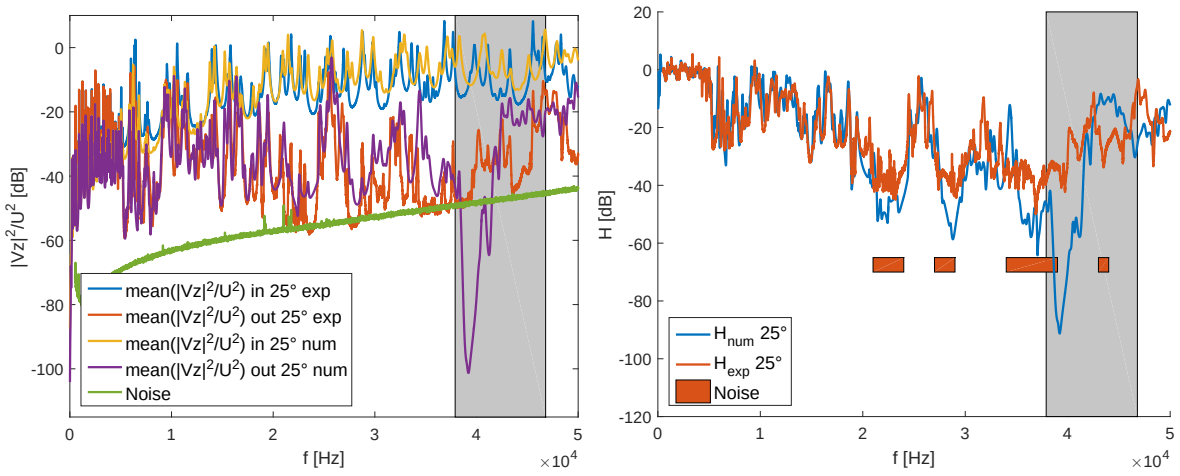

(a) (b)

Figure 9. a) Numerical and experimental frequency responses at ambient temperature $25°C$. Experimental average squared velocity amplitude $|Vz|^2$ for the input plate (IN) and the output plate (OUT) respectively in blue and red. Numerical ones respectively in yellow and purple. The green curve shows the noise measurement. The grey shape represents the bandgap predicted by the dispersion analyses at ambient temperature. b) Numerical and experimental transfer function IN/OUT at ambient temperature respectively in blue and red. Red areas show when velocity are in the same order of magnitude as noise.

The figure 9a is fully informed, an other representation is proposed. Transfer functions IN/OUT are presented in the figure9b. The transfer is defined, with experimental and numerical data, as follows:

$$H = 20 \times log_{10}\left(\frac{\Sigma^{out}(|Vz|^2/U^2)}{\Sigma^{in}(|Vz|^2/U^2)}\right), \tag{6}$$

where $\Sigma^{out}(|Vz|^2/U^2)$ and $\Sigma^{in}(|Vz|^2/U^2)$ are, respectively, the average squared velocity amplitude $|Vz|^2$ for the input plate (IN) and the output plate (OUT).

Red areas show when velocity are in the same order of magnitude as noise. Overall results except in areas where the measurement is close to ambient noise. Our numerical model is pretty representative, however the bandgap is not clearly observed in the experiments.

Figure 10 presents numerical and experimental frequency responses at $90°C$. Curves need to be compared by pair (yellow-blue and purple-red). Yellow and blue curves corresponds, respectively, to experimental and numerical average squared velocity amplitude $|Vz|^2$ for the input plate (IN). Purple and red curves corresponds, respectively, to experimental and numerical average squared velocity amplitude $|Vz|^2$ for the output plate (OUT). A good coherence is observed between the numerical and experimental results.

The effect related to the periodicity is no longer observed at this temperature. The aluminum pillars are completely decoupled from the plate and the polymer still plays a damping role. Frequency response functions are smoothed at this temperature.

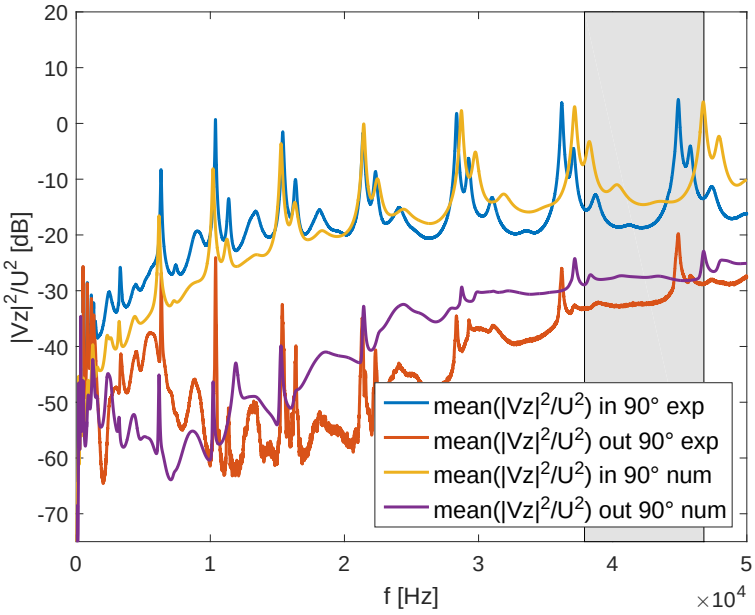

Figure 10. Numerical and experimental frequency responses at $90°C$. Experimental average squared velocity amplitude $|Vz|^2$ for the input plate (IN) and the output plate (OUT) respectively in blue and red. Numerical ones respectively in yellow and purple. The smooth grey shape represents the bandgap predicted by the dispersion analyse at ambient temperature.

3.4 Conclusion

In this article, numerical tools for the dispersion analysis in periodic damped structures are used, with a focus on the ability of the "Shift cell operator" method to deal with the dissipative behaviour of the system. An adaptive metamaterial mixing aluminum with a highly dissipative polymer interface is designed. The mechanical properties of the polymer depend on the frequency and the temperature, they change radically at the glass transition. The viscoelastic behavior of tBA/PEGDMA is approximated by a fractional Zener model. A 3D finite element model of the metamaterial elementary cell is designed for dispersion analysis using the "Shift cell operator" method. In order to validate the design and adaptability of the metamaterial, a complete 3D model integrating an interface composed of a distributed set of unit cells is presented. Different operating temperatures are studied. After this step, a comparison between the simulation results of the tunable structure and the experimental results is presented. Two states are obtained by changing the temperature of the polymer interface to ambient temperature, the bandgap predicted by the dispersion diagram is visible around the selected frequency. After the glass transition temperature, the metamaterial tends to behave like a homogeneous plate. A remark may be made on the experimental measurements. Indeed, the experimental facilities are well suitable for the resonance measurement, the amplitude is maximum, the signal-noise ratio is large. In our case, bang gaps are interesting where the vibration level is very low, approaching zero displacement, and therefore confuses with the measurement noise.

ACKNOWLEDGMENTS

This work was financed by The French National Research Agency under grant number ANR-12-JS09-008-COVIA. It has been performed in cooperation with the Labex ACTION program (ANR-11-LABX-0001-01).

REFERENCES

[1] Brillouin, L., [*Wave propagation in periodic structures*], Dover Publication (1953).

[2] Hussein, M., Leamy, M., and Ruzzene, M., "Dynamics of phononic materials and structures: Historical origins, recent progress, and future outlook," *Applied Mechanics Reviews* **66**(4), 040802 (2014).

[3] Shan, S., Kang, S., Zhao, Z., Fang, L., and Bertoldi, K., "Design of planar isotropic negative poissons ratio structures," *Extreme Mechanics Letters* **4**, 96–102 (2015).

[4] Slann, A., White, W., Scarpa, F., Boba, K., and Farrow, I., "Cellular plates with auxetic rectangular perforations," *physica status solidi (b)* **252**(7), 1533–1539 (2015).

[5] Billon, K., Zampetakis, I., Scarpa, F., Ouisse, M., Sadoulet-Reboul, E., Collet, M., Perriman, A., and Hetherington, A., "Mechanics and band gaps in hierarchical auxetic rectangular perforated composite metamaterials," *Composite Structures* **160**, 1042–1050 (2017).

[6] Joannopoulos, J., Johnson, S., Winn, J., and Meade, R., [*Photonic crystals: molding the flow of light*], Princeton university press (2011).

[7] Butaud, P., *Contribution à l'utilisation des polymères à mémoire de forme pour les structures à amortissement contrôlé*, PhD thesis (2015).

[8] Butaud, P., Foltête, E., and Ouisse, M., "Sandwich structures with tunable damping properties: On the use of shape memory polymer as viscoelastic core," *Composite Structures* **153**, 401–408 (2016).

[9] Collet, M., Ouisse, M., Ruzzene, M., and Ichchou, M., "Floquet–bloch decomposition for the computation of dispersion of two-dimensional periodic, damped mechanical systems," *International Journal of Solids and Structures* **48**(20), 2837–2848 (2011).

[10] Moiseyenko, R. and Laude, V., "Material loss influence on the complex band structure and group velocity in phononic crystals," *Phys. Rev. B* **83**(6), 064301 (2011).

[11] Laude, V., Escalante, J., and Martínez, A., "Effect of loss on the dispersion relation of photonic and phononic crystals," *Physical Review B* **88**(22), 224302 (2013).